Arch. Metall. Mater. **68** (2023), 3, 1143-1149

DOI: https://doi.org/10.24425/amm.2023.145486

K. GLOWKA[1], M. ZUBKO[1,2*], K. PIOTROWSKI[1], P. ŚWIEC[1], K. PRUSIK[1], R. ALBRECHT[1], D. STRÓŻ[1]

MICROSTRUCTURE AND SELECTED MECHANICAL PROPERTIES OF $Cr_{25}Zr_{25}Co_{20}Mo_{15}Si_{10}Y_5$ AND $Cr_{25}Co_{25}Zr_{20}Mo_{15}Si_{10}Y_5$ MULTICOMPONENT ALLOYS

In the presented work, two multicomponent $Cr_{25}Zr_{25}Co_{20}Mo_{15}Si_{10}Y_5$ and $Cr_{25}Co_{25}Zr_{20}Mo_{15}Si_{10}Y_5$ alloys were produced from bulk chemical elements using the vacuum arc melting technique. X-ray diffraction phase analysis was used to determine the phase composition of the obtained materials. Microstructure analysis included scanning electron microscopy and energy dispersive X-ray spectroscopy techniques. The studies revealed the presence of multi-phase structures in both alloys. Elemental distribution maps confirmed the presence of all six alloying elements in the microstructure. The segregation of chemical elements was also observed. Microhardness measurement revealed that both alloys exhibited microhardness from 832(27) to 933(22) HV1.

Keywords: Multicomponent Alloys; X-ray diffraction; Electron Microscopy; Microstructure; Microhardness

1. Introduction

High entropy alloys (HEAs) have recently gained much research interest worldwide. This group of materials belongs to a new class of engineering materials – classified as multi-principal elemental alloys (MPEAs) [1]. It should be underlined that the first literature-reported five-elemental, equiatomic HEA composition was published by Cantor et al. in 2004 [2]. High entropy alloys can be defined using chemical composition and/or configurational entropy (ΔS_{conf}) approach. Following chemical composition-based definition, HEAs are defined as *"materials containing at least five alloying elements in equi- or near-equiatomic ratios"* [3]. Additionally, for near-equiatomic compositions, *"the concentration of alloying elements should be in the range from 5 to 35 at. %"*[3]. The configurational entropy-based definition of HEAs includes *"materials exhibiting configurational entropy at a random state ≥ 1.5·R (where: R is a gas constant) wherever if the materials are single-phase or multi-phase at the room temperature"* [3].

Exhaustive studies of high entropy materials showed that HEAs present a high potential for industrial applications due to their improved properties compared to conventional alloys. Based on the literature-described data, a wide range of applications could be proposed, such as the storage of liquefied gases and cryogenic temperature applications (Cantor's alloy – Cr-Mn-Fe-Co-Ni) [4]. Due to high melting temperatures of alloying elements such as Ta, W, and V, HEAs exhibit a high potential ability to replace the Ti-based alloys in manufacture of gas turbine compressor components in aircraft engine, for example, Ta-Nb-Hf-Zr-Ti [5]. For special applications such as in the nuclear industry, the Fe-Ni-Mn-Cr composition proposed by Li et al. could be used due to the high resistance to radiation damage [5]. Furthermore, due to the presence of biocompatible alloying elements, high entropy alloys could also be applied as materials for biomedical applications [6]. Additionally, the particular group of high entropy alloys can exhibit shape memory effects, such as $(TiZrHf)_{50}Ni_{25}Co_{10}Cu_{15}$ and NiTiTaCoCu HEAs, due possibility of the presence of thermoelastic martensitic transformation [7-9].

It is well known that the chemical composition and cooling rate during the fabrication process determine the properties of studied materials in an as-cast state. Hume-Rothery (H-R) rules are fundamental to describe the formation of solid solutions (SS) for binary alloys. However, for HEAs, solid solution predictions could also be helpful in designing the chemical composition process. The studies of high entropy alloys revealed that the H-R rules could also be applied for HEAs, such as atomic size mismatch – δ and mixing enthalpy (ΔH_{mix}) [10,11]. The atomic size mismatch parameter described the differences between the alloying elements based on the atomic radii of elements (r_i). It was shown that the single-phase structure in HEAs was formed

[1] UNIVERSITY OF SILESIA IN KATOWICE, INSTITUTE OF MATERIALS ENGEENERING, CHORZÓW, POLAND
[2] UNIVERSITY OF HRADEC KRÁLOVÉ, DEPARTMENT OF PHYSICS, HRADEC KRÁLOVÉ, CZECH REPUBLIC
* Corresponding author: maciej.zubko@us.edu.pl

for δ in the 0 ÷ 5% range [11]. For higher values of atomic mismatch parameters, lattice distortion contributed to the formation of muti-phase or amorphous structures. The mixing enthalpy parameter (ΔH_{mix}) described the mixability/solubility of the chemical elements and also contributed to the phase formation after the solidification process. It should be noticed that single-phase structures are mainly formed for ΔH_{mix} in the $-15 \div 5$ kJ·mol^{-1} range. It was found that multi-phase structures are mainly formed for $\Delta H_{mix} > 5$ kJ·mol^{-1}. On the other hand, $\Delta H_{mix} < -15$ kJ·mol^{-1} favours the presence of amorphous structures [11].

It should be also underlined that the formation of the amorphous structure can be suggested according to the Inoue rules [12]. Preliminary studies of Inoue rules included bulk metallic glasses, however, it was revealed that these rules could also be adopted for multicomponent alloys [12]. Inoue's rules published in 2000 included: (1) the alloy system contains at least three chemical elements, (2) the mixing enthalpy (ΔH_{mix}) among the principal elements has a large negative value, and (3) the atomic size differences (δ) among the alloying elements should be higher than 12% [12].

Usually, amorphous alloys are created after reaching the critical cooling rate (CCR) [13]. Fabrication methods must be chosen to reach the CCR to obtain fully amorphous alloys. Literature data revealed that the critical cooling rate in the range $10^5 \div 10^6$ K·s^{-1} could be enough to produce fully amorphous materials [13]. In the literature, it was reported that manufacturing methods such as melt spinning (MS) or suction casting (SC) methods ensured reaching the CCR for various alloys [14-16]. The examples of literature-described amorphous high entropy alloys produced via MS or SC include Fe-Mn-Co-Cr-Ni [17], Ti-Ni-Si-Cr-Co-Al [18], Gd-Tm-Er-Co-Al [19], Hf-Nb-Ta-Ti-Zr [20], Fe-Co-Cr-Ni-Zr [21]. Amorphous high entropy alloys (AHEAs) could be classified as an interesting group of HEAs due to the possibility of developing chemical compositions and fabrication methods to obtain fully amorphous materials. However, based on the literature data, AHEAs are mainly produced using melt spinning or suction casting methods, which ensure the reach of CCR [14,22]. Moreover, amorphous high entropy materials can also reveal brittleness and insufficient properties, such as low plasticity at room temperature (V-Nb-Mo-Ta-W) [23]. However, there is still a need to design new AHEAs compositions produced by modern methods. Additionally, the development of fabrication methods could contribute to fill the knowledge gap of amorphous high entropy materials.

The main aim of the presented work was to design multicomponent alloys with high atomic size differences (δ) and significant negative mixing enthalpy (ΔH_{mix}) of alloying elements following the Inoue rules of obtaining amorphous alloys in an as-cast state (immediately after the vacuum arc melting). Furthermore, Si and Y chemical elements were chosen due to their amorphization ability and high atomic radii differences. To our best knowledge, producing amorphous multicomponent alloys using the vacuum arc melting technique could contribute to developing of fabrication methods. Moreover, both studied muticomponent compositions, $Cr_{25}Zr_{25}Co_{20}Mo_{15}Si_{10}Y_5$ and $Cr_{25}Co_{25}Zr_{20}Mo_{15}Si_{10}Y_5$ (at. %), were not described previously in the literature. The aim of the undertaken work was to investigate the microstructure, selected mechanical properties and the possibility of amorphous structure formation of the proposed alloys.

2. Materials and methods

Six elemental multicomponent $Cr_{25}Zr_{25}Co_{20}Mo_{15}Si_{10}Y_5$ (denoted as Sample 1) and $Cr_{25}Co_{25}Zr_{20}Mo_{15}Si_{10}Y_5$ (at.%) (denoted as Sample 2) alloys were produced from bulk elements with purity >99.5%. In order to remove the self-passivated oxygen layer, all bulk elements were ground using SiC grinding paper with P360. In the next step, alloying elements were precisely weighted using Radwag AS 60/220/C/2 laboratory weight. 5 g melting buttons were produced (diameter of the buttlo was approximately 1.3 mm) via the vacuum arc melting technique in an Ar atmosphere (chamber pressure of 1.2 bar). High-purity Ti-getter was used to capture residual gases in the chamber. Both samples were remelted five times and mixed in the liquid state for 180 s to achieve homogeneous distribution of alloying elements. No further thermal treatment was performed – the alloys were examined in the as-cast states. Both studied alloys were embedded into electron-conductive resin. As-embedded samples were further grinded using SiC grinding papers (grit from 320 to 2400). 6 μm, 3 μm, and 1 μm diamond suspension were used to polish the produced samples. Final polishing was performed using colloidal silica dioxide (SiO_2) OP-S suspension with 0.04-μm particle size.

X-ray powder diffraction (XRD) measurements were performed using Philips X'Pert PW 3040/60 diffractometer with Cu anode ($Cu_{K\alpha} - \lambda = 1.54056$ Å) working at an electric current of 30 mA, voltage of 40 kV, equipped with high-speed linear X'Celerator detector. X-ray diffraction patterns were collected using θ-θ geometry in the "step scanning" method with a 0.04° step and a counting time of 12 s/step in the angular range of $2\theta = 10 \div 140°$. The XRD phase analysis was performed using the International Centre for Diffraction Data (ICDD) PDF-4 database reference standards.

Microstructure analysis was performed using a JEOL JSM-6480 scanning electron microscope (SEM) working with the accelerating voltage of 20 kV and equipped with the Energy Dispersive X-ray Spectroscopy (EDS) detector from IXRF.

Microhardness measurements were carried out using Micro-Vickers tester 401MVD, equipped in ~136° pyramidal Vickers tip, under the load of 1 kg (HV 1) and dwell time of 10 s.

3. Results and Discussion

3.1. Phase formation predictions for studied alloys

As mentioned above, atomic size mismatch, mixing enthalpy, and Inoue rules were indicative for the selection of the presented chemical compositions of the studied alloys. These

TABLE 1

Thermodynamical parameters for the studied alloy: atomic size mismatch – δ, mixing enthalpy – ΔH_{mix}, mixing entropy (ΔS_{mix}), Valence Electron Concentration (VEC) and Zhang parameter (Ω) [25]

	δ [%]	ΔH_{mix} [kJ/mol]	ΔS_{mix} [J·(mol·K)$^{-1}$]	VEC	Ω	References
$Cr_{25}Zr_{25}Co_{20}Mo_{15}Si_{10}Y_5$ (Sample 1)	13.45	–31.36	13.97	5.75	0.95	Presented work
$Cr_{25}Co_{25}Zr_{20}Mo_{15}Si_{10}Y_5$ (Sample 2)	13.18	–30.32	13.97	6.00	0.97	Presented work
$Co_{15}Cr_{15}Mo_{25}Si_{15}Y_{15}Zr_{15}$	15.44	–29.49	14.71	5.40	1.08	[24]

mentioned parameters were selected in a regime that could lead to the formation of an amorphous phase after solidification. Both chemical compositions of the studied multicomponent alloys, $Cr_{25}Zr_{25}Co_{20}Mo_{15}Si_{10}Y_5$ and $Cr_{25}Co_{25}Zr_{20}Mo_{15}Si_{10}Y_5$, met the Inoue rules for amorphous phase formation. Above-described thermodynamical parameters for the studied composition were compared with literature-reported $Co_{15}Cr_{15}Mo_{25}Si_{15}Y_{15}Zr_{15}$ alloy [24] and are shown in TABLE 1.

3.2. X-ray Diffraction phase analysis of studied alloys

For both studies, Sample 1 and Sample 2, collected and indexed experimental X-ray diffraction patterns are presented in Fig. 1.

XRD phase analysis of both studied compositions revealed the presence of multi-phase structures. For both Sample 1 and Sample 2, the dominant phase was the structure similar to the ternary $CoMo_3Zr_2$ (ICDD 01-082-6072, hexagonal – space group $P6_3/mmc$) phase. The lattice parameters reported by ICDD were as follows: $a_0 = 5.0190$ Å and $c_0 = 8.2040$ Å. For both the studied multicomponent compositions, the second identified phase was a structure similar to the binary Si_3Y_5 (ICDD 04-003-3406) with a $P6_3/mcm$ space group as the above-described phase and lattice parameters $a_0 = 8.4230$ Å and $c_0 = 6.3540$ Å. The presence of the Si_3Y_5 phase was also literature-reported for Co-Cr-Mo-Si-Y-Zr high entropy alloy [24]. XRD phase analysis for both multicomponent alloys also revealed the presence of structures similar to pure Si (ICDD 04-002-2831), representing cubic crystal structures, with $Fd\bar{3}m$ space group. The ICDD lattice parameters were $a_0 = 5.2680$ Å. The content of the silicon phase in both studied samples is very low. For Sample 1, additionally, the presence of the fourth phase with a structure similar to pure Mo (ICDD 00-042-1120), with $Im\bar{3}m$ space group was identified. The ICDD lattice parameters were $a_0 = 3.1472$ Å. For Sample 1 and Sample 2 XRD phase analysis was correlated with SEM-EDS chemical composition analysis (see TABLE 3 and TABLE 4), where the presence of Co, Mo, Si, Y, and Zr-enriched phases were observed. However, based on the chemical composition analysis, pure Si has not been observed in the microstructure. Collected data of XRD phase analysis for both studied alloys are presented in TABLE 2.

The diffraction peaks position was analyzed for both the studied multicomponent materials in comparison to the position suggested by the ICDD standards. The detailed analysis of the recorded diffraction patterns showed that the 2θ peak position varies slightly from the ICDD-described location. It indicates that the lattice parameters are slightly different from the theoretical ones, contributing to the contraction and expansion of unit cell parameters. It is highly probable that the highest atomic radii of Y ($r_i = 1.802$ Å) and the lowest atomic radii of Si ($r_i = 1.153$ Å) could favour the expansion and contraction of unit cell parameters, respectively [24]. Detailed studies for confirmation of the identified phases using transmission electron microscopy (TEM) will be undertaken in future work.

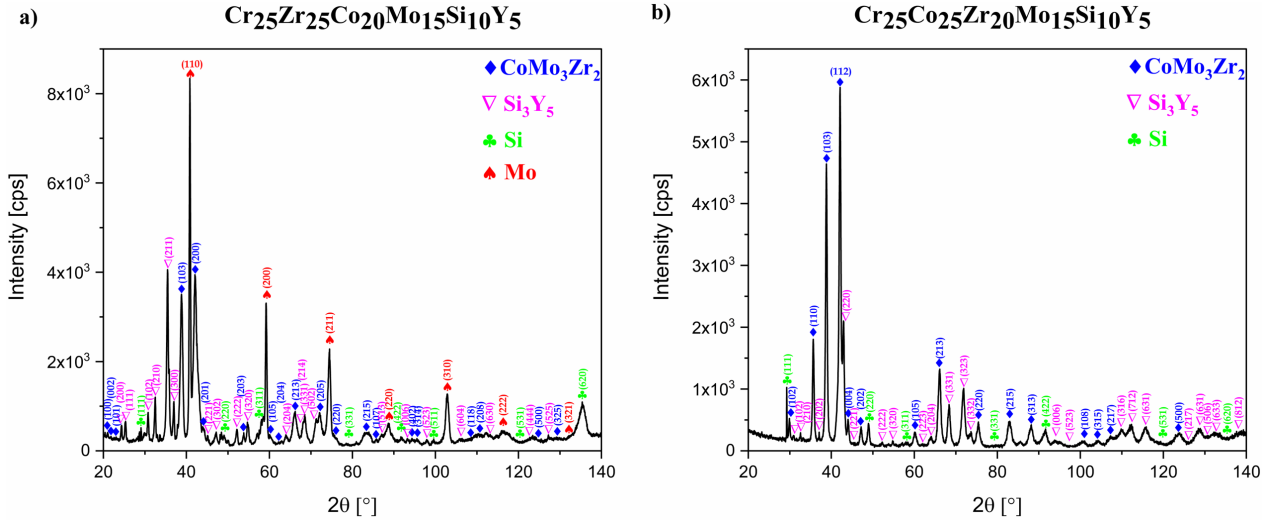

Fig. 1. Indexed X-ray diffraction patterns for a) $Cr_{25}Zr_{25}Co_{20}Mo_{15}Si_{10}Y_5$ and b) $Cr_{25}Co_{25}Zr_{20}Mo_{15}Si_{10}Y_5$ multicomponent alloys

TABLE 2

XRD data from ICDD for both studied multicomponent alloys

Sample	Sample 1				Sample 2		
Phase	$CoMo_3Zr_2$	Si_3Y_5	Si	Mo	$CoMo_3Zr_2$	Si_3Y_5	Si
Crystallographic system	Hexagonal		Cubic		Hexagonal		Cubic
Space group	$P6_3/mmc$	$P6_3/mcm$	$Fd\bar{3}m$	$Im\bar{3}m$	$P6_3/mmc$	$P6_3/mcm$	$Fd\bar{3}m$
ICDD	01-082-6072	04-003-3406	04-002-2831	00-042-1120	01-082-6072	04-003-3406	04-002-2831

3.3. Microstructure analysis of studied alloys

In order to study the microstructure of the obtained alloys, SEM observations have been performed. Backscattered electrons (BSE) images of Sample 1 and Sample 2 are presented in Fig 2.

Microstructure analysis confirmed the presence of multi-phase structures revealed during XRD phase analysis. The observed regions with differences in contrast, corresponding to the differences in the chemical compositions, were denoted as Phase 1, Phase 2, and Phase 3 for Sample 1 and Phase 1 and

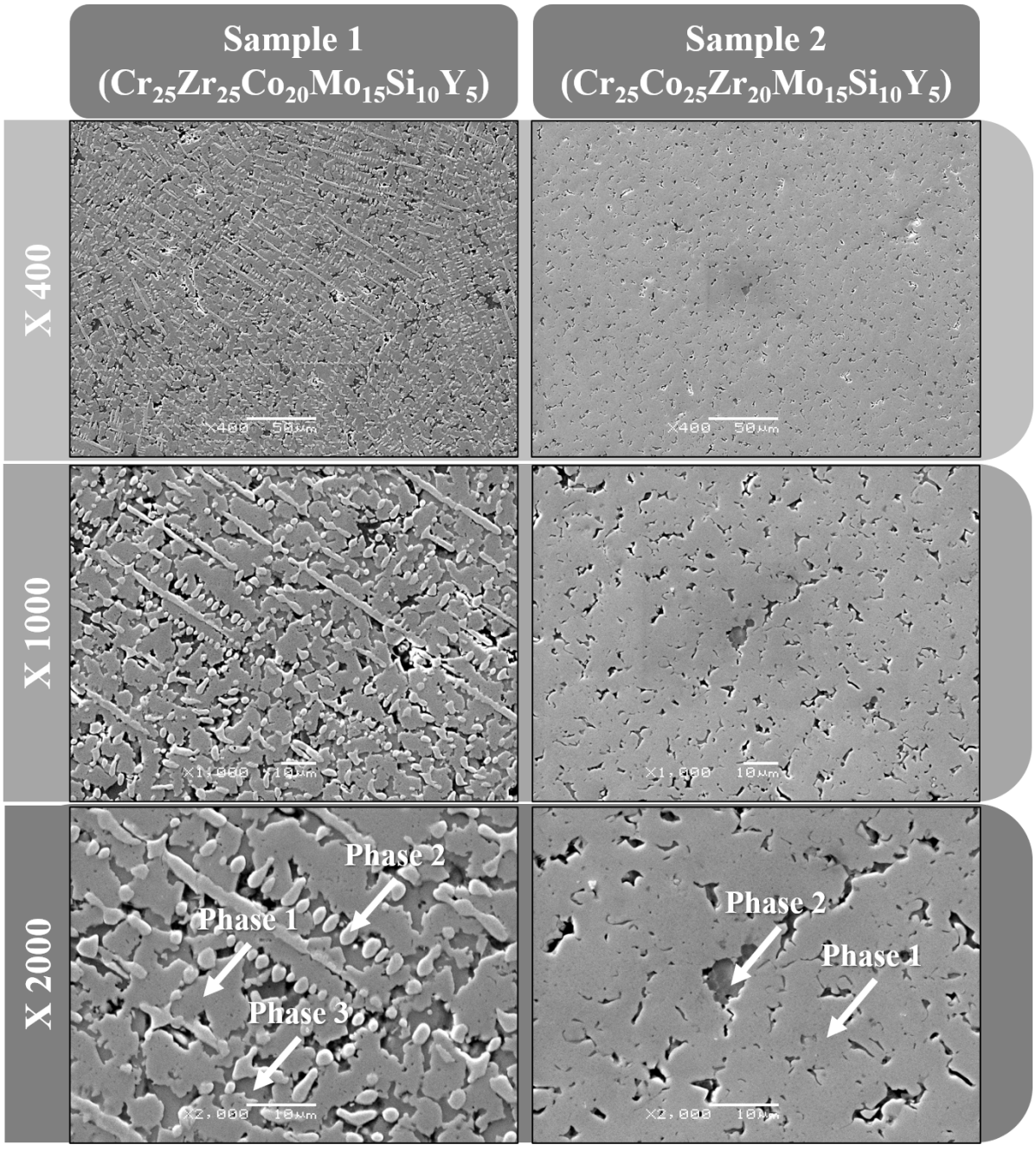

Fig. 2. SEM-BSE microstructure images with assigned phases for Sample 1 and Sample 2

Phase 2 for Sample 2, respectively. Furthermore, SEM microstructure images also showed the presence of small micropores.

In order to investigate the chemical compositions of the identified phases, SEM-EDS studies have been performed. For both studied multicomponent materials, the chemical composition analysis was performed based on the 40 measurements for each phase. The results of SEM-EDS chemical compositions are presented in TABLE 3 for Sample 1 and TABLE 4 for Sample 2, respectively. Moreover, obtained results were compared with the nominal chemical compositions of both studied alloys.

TABLE 3

SEM-EDS average chemical composition analysis for Sample 1

Sample 1						
	Elements and average at. %					
	Co	Cr	Mo	Si	Y	Zr
Nominal	20	25	15	10	5	25
Phase 1	21.6(4)	18.8(5)	11.0(5)	14.1(1)	1.9(1)	32.6(3)
Phase 2	4.0(1)	8.2(1)	86.6(2)	1.0(1)	0.0(0)	0.3(1)
Phase 3	4.5(2)	3.8(1)	2.2(1)	26.7(2)	58.6(5)	4.2(2)

TABLE 4

SEM-EDS average chemical composition analysis for Sample 2

Sample 2						
	Elements and average at. %					
	Co	Cr	Mo	Si	Y	Zr
Nominal	25	25	15	10	5	20
Phase 1	13.9(2)	21.0(4)	20.5(8)	7.0(1)	4.5(5)	33.2(1)
Phase 2	14.7(3)	17.7(4)	15.1(9)	10.8(3)	15.9(6)	25.9(2)

For Sample 1, it was revealed that Phase 1 was mainly Co, Cr, Mo, Si and Zr-enriched. On the other hand, this phase was Y-depleted. For Phase 2, SEM-EDS analysis showed the enrichment mainly in Mo with a small concentration of Cr and Co. It is probable that low mixing enthalpy of Mo with other alloying elements contributes to the formation of Mo-enriched phases. Moreover, the presence of a phase with a high concentration of Mo could correspond to the highest melting point of this element in comparison to other chemical elements. On the other hand, Phase 3 for this sample was Si and Y-enriched, which could correspond to the Si_3Y_5 phase, confirmed by XRD phase analysis. Based on the SEM-EDS chemical composition analysis, it could be concluded that Si and Y exhibit good mixability. Moreover, the enrichment in both Si and Y chemical elements was also observed for the literature-reported Co-Cr-Mo-Si-Y-Zr alloys [24].

For Sample 2, the enrichment in Zr, Cr, and Mo was observed for Phase 1. On the other hand, chemical composition analysis revealed the enrichment in Zr, Cr, Y, and Mo for Phase 2.

In order to confirm the elemental segregation in the microstructures of both studied alloys, the elemental distribution maps (EDM) have been recorded (Fig. 3). It should be underlined that EDM confirmed the above-described EDS chemical composition analysis.

3.4. Microhardness measurements of studied alloys

Microhardness measurements were performed to determine the mechanical properties of the studied multicomponent alloys. Microhardness was determined based on 20 indents from the central part of both samples. Due to the micrometric size of Vickers tip, presented microhardness are the average values from all identified phases. Obtained results were compared with literature-reported high entropy and multicomponent alloys and are presented in TABLE 5.

TABLE 5

Microhardness of studied high entropy alloys in comparison to literature-reported HEAs and multicomponent materials

Chemical composition	Microhardness [HV1]	References
Nb-24Ti-18Si-5Al-5B-5Cr-6Ta	1480	[26]
Sample 2 ($Cr_{25}Co_{25}Zr_{20}Mo_{15}Si_{10}Y_5$)	933(22)	Present work
Sample 1 ($Cr_{25}Zr_{25}Co_{20}Mo_{15}Si_{10}Y_5$)	832(27)	Present work
Fe-Al35-Si5	819	[27]
Ti-Zr-Al-Nb-Co	769	[28]
Co-Cr-Fe-Ni-Nb	620	[29]
HfMo0.5NbTiV0.5Si0.7	612	[30]
Ni-Cr-B-Si	580	[31]
$Ti_{20}Ta_{20}Nb_{20}(ZrHf)_{10}Mo_{20}$	557	[32]
Ti-Nb-Ta-Zr-W	556	[33]
Co-Cr-Mo-Si	515	[34]
$Ti_{20}Ta_{20}Nb_{20}(ZrHf)_{12.5}Mo_{15}$	505	[32]
$Ti_{20}Ta_{20}Nb_{20}(ZrHf)_{20}$	475	
$Ti_{20}Ta_{20}Nb_{20}(ZrHf)_{17.5}Mo_5$	469	
Ti-Nb-Ta-Zr-V	430	[33]
$Ti_{20}Ta_{20}Nb_{20}(ZrHf)_{15}Mo_{10}$	427	[32]
Cu-Ni-Si	280	[34]
Al-Si-Cu-Fe-Mg	270	[35]
Al-Mg-Si	110	[36]

Microhardness measurements revealed that both studied compositions exhibited high microhardness equal to 832(27) HV1 for Sample 1 and 933(22) HV1 for Sample 2, respectively. Moreover, the microhardness of investigated materials was much higher in comparison to literature-reported HEAs such as refractory Ti-Nb-Ta-Zr-V and Ti-Nb-Ta-Zr-W [33], Co-Cr-Fe-Ni-Nb [29], Ti-Zr-Al-Nb-Co [28] high entropy alloys. Microhardness measurements also revealed that both studied alloys exhibited higher microhardness in comparison to Mo-containing, six-elemental Ti-Ta-Nb-Zr-Hf [32], and Si and Y-containing Fe-Al35-Si5 alloy [27].

The changes in chemical compositions of the studied alloys probably contributed to the increase of microhardness in comparison to literature-reported HEAs and multicomponent materials. Furthermore, it was also literature-described that the addition of Si and Y also increased the microhardness of reported materials [37], [38]. Moreover, XRD phase and SEM-EDS chemical composition analysis for Samples 1 and Sample 2 revealed the

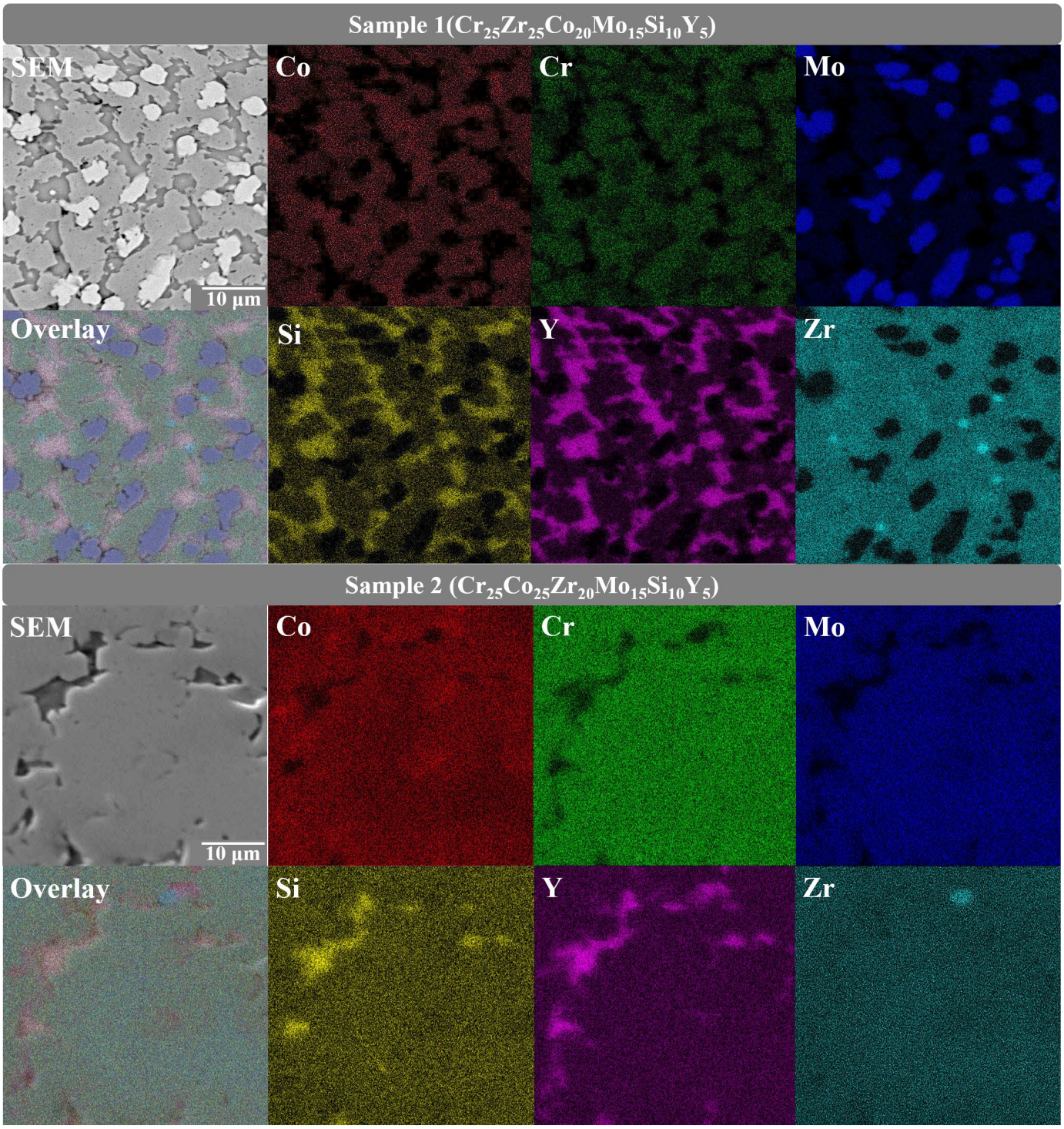

Fig. 3. SEM-EDS elemental distribution maps for studied Sample 1 and Sample 2

presence of structures corresponding to Si_3Y_5 phases and the presence of Si and Y-enriched regions, which could significantly increase the microhardness of studied multicomponent alloys.

The drawback of the potential application ability of studied alloys could correspond to the presence of multi-phase structures. However, the development in fabrication methods, such as melt spinning or suction casting, could contribute to obtaining fully amorphous structures (to reach a critical cooling rate) in an as-cast state. Moreover, further changes in chemical compositions in order to increase the atomic size mismatch (δ) and drastically decrease the mixing enthalpy (ΔH_{mix}) of the alloying elements could also contribute to obtaining amorphous structures.

4. Conclusions

Two six-elemental multicomponent $Cr_{25}Zr_{25}Co_{20}Mo_{15}Si_{10}Y_5$ and $Cr_{25}Co_{25}Zr_{20}Mo_{15}Si_{10}Y_5$ (at. %) alloys were designed and vacuum arc melted. The chemical compositions were chosen to obtain high atomic radii differences, large, negative mixing

enthalpy and reach the Inoue rules of an amorphous phase formation. XRD and SEM analysis revealed the presence of multi-phase structures in both studied multicomponent materials. Furthermore, identified phases represented hexagonal and cubic crystal structures. Moreover, all phases exhibited differences in the space groups and lattice parameters. Microstructure, SEM-EDS chemical composition, and SEM-EDM confirmed the elemental segregations in the microstructure of the studied materials. Due to the presence of Si and Y-enriched phases, both alloys exhibited much higher microhardness compared to literature-reported high entropy alloys and muticomponent alloys. From the performed measurements, we could not confirm the presence of amorphous phases in the studied materials. Further TEM observation would be needed in order to examine the structure of the studied materials. It is probable that like in a similar composition $Co_{15}Cr_{15}Mo_{25}Si_{15}Y_{15}Zr_{15}$ [24] small amorphous regions could be present. The performed observations indicate that the Inoue rules can not be the only indication of obtaining amorphous phases in multicomponent alloys without achieving critical cooling rates.

REFERENCES

[1] J.W. Yeh, High-Entropy Alloys: Fundamentals and Applications, Springer International Publishing (2016).

[2] B. Cantor, I.T.H. Chang, P. Knight, A.J.B. Vincent, Mater. Sci. Eng. A, (2004). DOI: https://doi.org/10.1016/j.msea.2003.10.257

[3] J.W. Yeh et al., Adv. Eng. Mater. (2004). DOI: https://doi.org/10.1002/adem.200300567.

[4] B. Gludovatz, A. Hohenwarter, D. Catoor, E.H. Chang, E.P. George, R.O. Ritchie, Science (2014). DOI: https://doi.org/10.1126/science.1254581

[5] W. Li, D. Xie, D. Li, Y. Zhang, Y. Gao, P.K. Liaw Prog. Mater. Sci. (2021). DOI: https://doi.org/10.1016/j.pmatsci.2021.100777

[6] W. Yang, S. Pang, Y. Liu, Q. Wang, P.K. Liaw, T. Zhang, Intermetallics (2021). DOI: https://doi.org/10.1016/j.intermet.2021.107421

[7] C.H. Chen, Y.J. Chen, Scr. Mater. (2019). DOI: https://doi.org/10.1016/j.scriptamat.2018.11.023

[8] K. Glowka et al., Arch. Metall. Mater. (2019). DOI: https://doi.org/10.24425/amm.2019.127603

[9] K. Glowka et al. Arch. Metall. Mater. (2019). DOI: https://doi.org/10.24425/amm.2019.127614

[10] Y. Zhang, Y.J. Zhou, J.P. Lin, G.L. Chen, P.K. Liaw, Adv. Eng. Mater. (2008). DOI: https://doi.org/10.1002/adem.200700240

[11] Y.F. Ye, Q. Wang, J. Lu, C.T. Liu, Y. Yang, Mater. Today, (2016). DOI: https://doi.org/10.1016/j.mattod.2015.11.026

[12] A. Inoue, Acta Mater. (2000). DOI: 10.1016/S1359-6454(99)00300-6

[13] R. Fulchiron, I. Belyamani, J. U. Otaigbe, V. Bounor-Legaré, Sci. Rep. (2015). DOI: https://doi.org/10.1038/srep08369

[14] A.A. Shirzadi, T. Kozieł, G. Cios, P. Bała, J. Mater. Process. Technol. (2019). DOI: https://doi.org/10.1016/j.jmatprotec.2018.09.028

[15] R.C. Budhani, T.C. Goel, K.L. Chopra, Bull. Mater. Sci. (1982). DOI: https://doi.org/10.1007/BF02824962

[16] J.K. Carpenter P.H. Steen, J. Mater. Sci. (1992). DOI: https://doi.org/10.1007/BF00553859.

[17] L. Xiao, Z. Zheng, P. Huang, F. Wang, Scr. Mater. (2022). DOI: https://doi.org/10.1016/j.scriptamat.2021.114454

[18] S. Li, T. Yamaguchi, Surf. Coatings Technol. (2022). DOI: https://doi.org/10.1016/j.surfcoat.2022.128123

[19] M. Cai, Q. Luo, Q. Zeng, B. Shen, J. Magn. Magn. Mater. (2021). DOI: https://doi.org/10.1016/j.jmmm.2021.167817

[20] P. Hruška et al., J. Alloys Compd. (2021). DOI: https://doi.org/10.1016/j.jallcom.2020.157978

[21] C. Xie et al., J. Non. Cryst. Solids. (2019). DOI: https://doi.org/10.1016/j.jnoncrysol.2019.03.039

[22] A. Chrobak, M. Karolus, G. Haneczok, Solid State Phenom. (2010. DOI: https://doi.org/10.4028/www.scientific.net/SSP.163.233

[23] Y. Zhang et al., Prog. Mater. Sci. (2014). DOI: https://doi.org/10.1016/j.pmatsci.2013.10.001.

[24] K. Glowka et al., Metals (Basel). (2020). DOI: https://doi.org/10.3390/met10111456

[25] X. Yang, Y. Zhang, Mater. Chem. Phys. (2012). DOI: https://doi.org/10.1016/j.matchemphys.2011.11.021

[26] T. Thandorn, P. Tsakiropoulos, Materials (Basel) (2021). DOI: https://doi.org/10.3390/ma14247615

[27] P. Novák, Z. Barták, K. Nová, F. Průša, Materials (Basel) (2020). DOI: https://doi.org/10.3390/ma13030800

[28] X.J. Jiang et al., Mater. Lett. (2022). DOI: https://doi.org/10.1016/j.matlet.2021.131131

[29] B. Chanda, J. Das, J. Alloys Compd. (2022). DOI: https://doi.org/10.1016/j.jallcom.2022.163610

[30] Y. Liu et al., J. Alloys Compd. (2017). DOI: https://doi.org/10.1016/j.jallcom.2016.10.014

[31] J.M.S. de Sousa, A. de S.P. Pereira, M. Pereira, R.G.N. Silva, J. Laser Appl. (2020). DOI: https://doi.org/10.2351/7.0000099

[32] K. Glowka et al. Materials (Basel) (2022). DOI: https://doi.org/10.3390/ma15010393

[33] T. Nagase, M. Todai, P. Wang, S.-H. Sun, T. Nakano, Mater. Chem. Phys. (2022). DOI: https://doi.org/10.1016/j.matchemphys.2021.125409

[34] P. Tunthawiroon, A. Chiba, IOP Conf. Ser. Mater. Sci. Eng. (2019). DOI: https://doi.org/10.1088/1757-899X/635/1/012006

[35] S.-S. Ahn et al., Materials (Basel) (2018). DOI: https://doi.org/10.3390/ma11112150

[36] L. Giersberg, B. Milkereit, C. Schick, O. Kessler, Mater. Sci. Forum (2014). DOI: https://doi.org/10.4028/www.scientific.net/MSF.794-796.939

[37] R. Liu, J. Yao, Q. Zhang, M.X. Yao, R. Collier, J. Eng. Mater. Technol. (2016). DOI: https://doi.org/10.1115/1.4034075

[38] L.J. Zhang et al., Mater. Sci. Eng. A, (2018). DOI: https://doi.org/10.1016/j.msea.2018.04.058